Published in final edited form as:

Cancer Res. 2008 February 01; 68(3): 664–673. doi:10.1158/0008-5472.CAN-07-2615.

Modeling Genomic Diversity and Tumor Dependency in Malignant Melanoma

William M. Lin[1,3,5], **Alissa C. Baker**[1,3], **Rameen Beroukhim**[1,3,5], **Wendy Winckler**[1,3,5], **Whei Feng**[1,3,5], **Jennifer M. Marmion**[7], **Elisabeth Laine**[8], **Heidi Greulich**[1,3,5], **Hsiuyi Tseng**[1,3], **Casey Gates**[5], **F. Stephen Hodi**[1], **Glenn Dranoff**[1], **William R. Sellers**[1,6], **Roman K. Thomas**[9,10], **Matthew Meyerson**[1,3,4,5], **Todd R. Golub**[2,3,5], **Reinhard Dummer**[8], **Meenhard Herlyn**[7], **Gad Getz**[3,5], **Levi A. Garraway**[1,3,5]

[1]Department of Medical Oncology, Dana-Farber Cancer Institute, Harvard Medical School

[2]Department of Pediatric Oncology, Dana-Farber Cancer Institute, Harvard Medical School

[3]Department of Center for Cancer Genome Discovery, Dana-Farber Cancer Institute, Harvard Medical School

[4]Department of Pathology, Harvard Medical School, Boston, Massachusetts

[5]The Broad Institute of M.I.T. and Harvard

[6]Novartis Institutes for Biomedical Research, Cambridge, Massachusetts

[7]Cancer Biology Division, Wistar Institute, Philadelphia, Pennsylvania

[8]Department of Dermatology, University of Zurich Hospital, Zürich, Switzerland

[9]Max Planck Institute for Neurological Research with Klaus Joachim Zulch Laboratories of the Max Planck Society and the Medical Faculty of the University of Cologne

[10]Center for Integrated Oncology and Department I for Internal Medicine, University of Cologne, Cologne, Germany

Abstract

The classification of human tumors based on molecular criteria offers tremendous clinical potential; however, discerning critical and “druggable” effectors on a large scale will also require robust experimental models reflective of tumor genomic diversity. Here, we describe a comprehensive genomic analysis of 101 melanoma short-term cultures and cell lines. Using an analytic approach designed to enrich for putative “driver” events, we show that cultured melanoma cells encompass the spectrum of significant genomic alterations present in primary tumors. When annotated according to these lesions, melanomas cluster into subgroups suggestive of distinct oncogenic mechanisms. Integrating gene expression data suggests novel candidate effector genes linked to recurrent copy gains and losses, including both phosphatase and tensin homologue (PTEN)–dependent and PTEN-independent tumor suppressor mechanisms associated

Requests for reprints: Levi A. Garraway, Department of Medical Oncology, Dana-Farber Cancer Institute, D1542, Boston, MA 02115. Phone: 617-632-6689; levi_garraway@dfci.harvard.edu.

W.M. Lin and A.C. Baker contributed equally to this work.

Supplementary data for this article are available at Cancer Research Online (http://cancerres.aacrjournals.org/).

with chromosome 10 deletions. Finally, sample-matched pharmacologic data show that *FGFR1* mutations and extracellular signal–regulated kinase (ERK) activation may modulate sensitivity to mitogen-activated protein kinase/ERK kinase inhibitors. Genetically defined cell culture collections therefore offer a rich framework for systematic functional studies in melanoma and other tumors.

Introduction

The recognition that cancer is fundamentally a genetic disease (1, 2), combined with an expanding repertoire of targeted small molecules (3–7), provides grounds for optimism that genome-based therapeutics may ultimately prove broadly applicable to human cancer. However, rational use of targeted anticancer agents is often encumbered by an inability to identify a priori those tumors whose unique biology confers heightened susceptibility to a particular treatment. Toward this end, considerable insights into tumorigenesis have been derived from functional studies involving cultured human cancer cells (e.g., established cell lines, short-term cultures, etc.). Despite their limitations, cancer cell line collections whose genetic alterations reflect their primary tumor counterparts should provide malleable proxies that facilitate mechanistic dissection and therapeutic development. Indeed, matched genomic and experimental data from these models may refine hypothesis generation and reveal new insights, as evidenced by recent studies (8, 9). Such results can also be integrated with analogous data from clinical specimens to infer molecular subtypes and therapeutic vulnerabilities in tumors that manifest the relevant genomic changes (10–12).

When it escapes early detection, malignant melanoma usually becomes a highly lethal malignancy that is refractory to existing therapeutic avenues (13, 14). However, whereas many other solid tumors lack robust *in vitro* counterparts, melanoma offers an attractive experimental platform for systematic functional characterization of genomic aberrations in cancer. Melanoma cells from patients with advanced disease proliferate readily *in vitro*; thus, hundreds of “short-term” melanoma cultures and established cell lines have been generated (15–17). Melanoma short-term cultures have typically undergone a relatively small number of passages outside of the patient, and the majority of these lines proliferate readily under standard laboratory conditions. In principle, then, a cultured melanoma collection that reflects the diversity of genomic aberrations observed in primary melanomas should facilitate the characterization of critical and “druggable” effectors linked to key molecular lesions in this malignancy. Accordingly, in this study we have undertaken detailed genomic characterization and integrative analysis of a large cultured melanoma cell collection, thereby establishing a robust framework for systematic cancer gene discovery and tumor dependency characterization in this malignancy.

Materials and Methods

Cell culture and reagents.

Short-term melanoma cultures were selected from cryopreserved collections at the Wistar Institute (62 lines), the University Hospital of Zurich (24 lines), and the Dana-Farber Cancer Institute (37 lines). Established melanoma cell lines were kindly provided by Drs. David

Fisher (Dana-Farber Cancer Institute, Boston, MA), Frank Haluska (Tufts - New England Medical Center Cancer Center, Boston, MA), Susan Holbeck (National Cancer Institute, Bethesda, MD), and Neal Rosen (Memorial Sloan Kettering Cancer Center, New York, NY). All cell lines and short-term cultures were cultured in RPMI medium (MediaTech) supplemented with 10% fetal bovine serum (MediaTech), except for the Dana-Farber short-term cultures, which were cultivated in DMEM (MediaTech) supplemented with 10% serum. For some Wistar lines, tissue culture dishes were first coated with 1% porcine gel solution (Sigma) to enhance cell adherence.

High-density single-nucleotide polymorphism array hybridization.

Genomic DNA was prepared from near-confluent cells using the DNEasy Tissue Kit (Qiagen) according to the manufacturer's instructions. For highly pigmented cultures, 1:1 phenol-choloroform extractions were done before column purification. Single-nucleotide polymorphism (SNP) array data were generated using either the *Sty*I chip from the 500K Human Mapping Array set (70 samples; see Supplementary Table S1) or the *Xba*I chip from the 50K Human Mapping Array set (31 samples; Affymetrix, Inc.). Array experiments using 250 ng of genomic DNA were carried out in a 96-well format using a Biomek FX robot with dual 96 and span-8 heads (Beckman Coulter) and a GeneChip Fluidics Station FS450 (Affymetrix), as described in Supplementary Methods. After hybridization, microarrays were scanned using the GeneChip Scanner 3000 7G (Affymetrix) to generate .cel and .txt files. Subsequent data processing steps are detailed in Supplementary Methods.

High-throughput oncogene mutation profiling and DNA sequencing.

Genomic DNA was genotyped for 238 known mutations in 17 oncogenes as described previously (18). Alternatively, BRAF and NRAS mutations were determined by Sanger sequencing (Agencourt). Available samples were sequenced for phosphatase and tensin homologue (*PTEN*) coding and splice junction mutations using prevalidated exon primers (Agencourt) and analyzed with Mutation Surveyor software (SoftGenetics, LLC.).

Gene expression profiling.

RNA was purified by a TRIzol extraction protocol (Invitrogen), as described in Supplementary Methods. Affymetrix HT-HGU133A chips were used for gene expression profiling (19). Using 1.0 μg of RNA, synthesis of the cRNA target product, microarray hybridization, and scanning (Affymetrix HT scanner) were done in a 96-well plate format according to the manufacturer's protocols. Scanned data were processed using MAS 5.0 (Affymetrix) as described in Supplementary Methods.

Bacterial artificial chromosome array data processing.

Bacterial artificial chromosome (BAC) array comparative genomic hybridization (CGH) primary melanoma data (20) were downloaded from the GEO database (GSE2631). The genomic markers were converted from hg16 to hg17 using the UCSC genome browser.[11] Missing data were imputed using the mean of neighboring values. Log_2 ratio values were

[11] http://genome.ucsc.edu/cgi-bin/hgLiftOver

smoothed using the GLAD segmentation algorithm (21). BAC markers in regions of known copy number polymorphisms were removed[12] before downstream analysis.

Genomic Identification of Somatic Targets in Cancer analysis.

Details of the Genomic Identification of Somatic Targets in Cancer (GISTIC) algorithm are described elsewhere (22). Briefly, each SNP array or CGH data set is defined in terms of copy-number values for N markers along the genome in M tumor samples. To identify significant regions of amplification and deletion, the GISTIC algorithm considers both the frequency F of an amplification or deletion above (or below) a certain threshold defined by normal samples and the average amplitude of that alteration A beyond the threshold. Thereby, a genome significance score (G score) $G = F \times A$ is defined over N markers for all M samples. At each individual marker n, the computed metric g is compared with the null hypothesis—a background metric defined by permutation testing across all the markers. Correcting for multiple hypotheses, a false discovery rate (q value) is generated at each marker n, aggregating information from M samples. Using GLAD-segmented copy number data from each sample (21), the minimal common region of overlap is used to define boundaries of peaks in the distribution of q values. A “wide peak” boundary is determined by the samples remaining after leaving out the individual samples that define the borders of the “narrow peak.” This wide peak reduces the influence of individual samples in dictating peak borders. In Tables 1 and 2 the wide peak region is indicated.

Inference of loss of heterozygosity.

A Hidden Markov Model (dChipSNP, August 16, 2006 build) that considers haplotype information from a pool of normal samples was used to infer loss-of-heterozygosity (LOH) calls, as previously described (ref. 23; Supplementary Methods).

Hierarchical clustering using genomic alterations.

An input binary matrix was generated from the GISTIC algorithm (see above). For each lesion defined by GISTIC, a ”1” was assigned to a lesion i in a given sample j if the middle marker in the lesion i region exceeded the designated $\log_2$ ratio threshold of 0.3 for amplifications, or −0.3 for deletions. Otherwise, that cell ij was assigned a “0.” Hierarchical clustering (24) with Euclidean distance and complete linkage was applied to this matrix using the GenePattern software package (25).

Significance analysis of microarrays.

Significance analysis of microarray (SAM) was done using TIGR MeV 4.0[13] to identify differentially expressed genes associated with a broad copy number lesion (i.e., chromosome 10 copy number loss) or a more focal event (i.e., peak of a GISTIC lesion). For the chromosome 10 studies, samples were first ranked into three classes based on mean $\log_2$ copy number over the region. Thresholds were chosen based on the 33rd and 67th percentiles of the copy number distribution. Calculations were done with K-nearest

[12] http://projects.tcag.ca/variation/
[13] http://www.tm4.org/mev.html

neighbors (10 neighbors), 200 permutations, and the Tusher method (26) to select the minimum δ where the median number of false-positive genes is zero.

Pharmacologic growth inhibition assays.

Cultured melanoma cells were added to 96-well plates at 1,000 (A375 and MCF7) and 3,000 (all short-term melanoma cultures and the MALME 3M cell line) cells per well. Cells were allowed to adhere overnight, and medium containing serial dilutions of CI-1040 (from 100 to 1×10^{-6} μmol/L; WuXi PharmaTech) was added. Cells were incubated for 96 h, at which time cell viability was measured using the CellTiter-Glo viability assay (Promega). Viability was calculated as a percentage of untreated control values after background subtraction.

Western blotting and biochemical studies.

After cell lysis, Western blot analysis was done as described in Supplementary Methods.

Results

Systematic genomic analysis of cultured melanoma cells.

To enhance global knowledge of melanoma genomic alterations while also establishing a robust experimental system for downstream functional characterization, we generated comprehensive genomic data for 101 cultured melanoma cells, which included both "short-term" cultures derived primarily from metastatic foci (median, 9 passages *in vitro*; range, 5–51) and established melanoma cell lines (Supplementary Table S1). Chromosomal copy number and LOH alterations were examined using high-density SNP arrays (8, 27, 28), and the mutation status of 17 known oncogenes was interrogated by Sanger sequencing or a mass spectrometry–based mutation profiling approach described previously (18). Gene expression patterns were determined for 88 cultured melanoma lines and 5 normal melanocyte lines using a high-throughput microarray platform (ref. 19; Affymetrix; see Materials and Methods). Altogether, 123 cultured melanoma lines were examined by one or more of these platforms (Supplementary Table S1).

Next, we wished to identify which genetic changes represented statistically significant events (presumably enriched for driver alterations) in melanoma. To accomplish this, we used an algorithm termed Genomic Identification of Significant Targets in Cancer (GISTIC; refs. 22, 29). This method systematically computes a significance score at each locus across the genome using smoothed microarray/CGH copy number data based on the frequency and amplitude of each alteration (G score; see Materials and Methods). After permutation testing and multiple hypothesis correction, resulting false discovery rate–corrected P values are plotted as a function of chromosomal location. Significant genomic regions of gain or loss are denoted by peaks in the GISTIC plot; the underlying chromosomal regions may then be inspected for candidate target genes.

The GISTIC output revealed 14 major regions of significant copy number gain and 13 regions of significant copy number loss in the cultured melanoma collection (Fig. 1A and B; Tables 1 and 2). One of the most significant regions of copy gain was located on chromosome 7q34 (65% of samples; Fig. 1A). This locus harbors the *BRAF* oncogene,

which contains activating point mutations in 56% of samples in our study, consistent with previously reported frequencies of >50% in cutaneous melanomas (30). A co-occurrence of these two events (36 of 79 samples) suggests that mutated *BRAF* may also be amplified in melanoma, although this correlation did not reach statistical significance ($P = 0.14$, two-tailed Fisher's exact test). Additional prominent GISTIC copy gain peaks localized exquisitely to *MITF*, which is the master transcriptional regulator of melanocyte development and an amplified oncogene in 10% to 15% of melanomas (8), and to *CCND1*, a well-known oncogenic cell cycle regulator (Fig. 1A). The most prominent region of copy loss identified *CDKN2A*, an established melanoma tumor suppressor gene (ref. 31; Fig. 1B). Thus, GISTIC analysis afforded a robust and unbiased means to identify key genomic loci whose target genes may contribute importantly to melanoma biology.

"Cross-platform" analyses of melanoma tumor genomic DNA.

Given that the GISTIC algorithm computes genomic regions of significance using smoothed copy number data, we reasoned that this method might also facilitate systematic genomic studies of tumors whose chromosomal copy number data derive from distinct microarray platforms. To explore this possibility, we compared the GISTIC plots generated on 250K SNP arrays from 70 melanoma short-term cultures, 50K SNP arrays from 31 additional short-term cultures and cell lines, 33K tiling arrays from 45 independent cell lines (32), and BAC array CGH data derived from 70 primary cutaneous melanomas (ref. 20; see Materials and Methods; Fig. 1A and B; Supplementary Fig. S1). The resulting GISTIC plots were strikingly similar across all data sets, suggesting that this algorithm could extract essential tumor genomic information regardless of the platform used. To confirm these similarities, we carried out pairwise Pearson correlations between GISTIC significance values of cultured melanoma data, primary melanomas, and several additional solid tumor data sets whose chromosomal aberrations had previously been examined (Supplementary Table S2; see Supplementary Methods). Notably, GISTIC correlations between cultured melanoma cells and primary cutaneous melanomas from nonchronic sun-damaged skin were stronger than any other correlation observed among all pairs of primary tumor sets, approaching that of the positive control (see Supplementary Methods). Thus, the chromosomal regions of significance gleaned from GISTIC analyses were robust to the types of microarray platform variances common to cancer genomic data sets.

The genomic diversity of melanoma *in vitro* and *in vivo*.

Theoretically, cultured human cancer cell collections may represent a biased malignant subset that fail to encompass the pathophysiology relevant in primary tumors. To address this at a genomic level in cutaneous melanoma, we compared the genomic regions of significance found in cultured melanoma cells to those observed in primary tumors. As shown in Fig. 1A and B, the landscape of genomic alterations was strikingly similar between cultured cells and primary tumors, even with respect to subtle contours within the GISTIC plots. Some significant alterations present in cultured cells were absent in primary tumors [e.g., gains on chromosome 3p14 (*MITF*) and chromosome 15q, and a region of loss on 4q]; in most cases, these were attributable to low BAC clone coverage in the primary tumor data. Conversely, a single peak of chromosomal deletion centered at 13q33 exhibited reduced prominence in cultured cells compared with primary tumors

(Fig. 1B). Interestingly, the underlying 3.2-Mb locus spanned the *ERCC5* excision repair gene, and this deletion showed increased significance in primary melanomas from chronic sun-damaged skin (ref. 20; Supplementary Fig. S2). These findings raised the possibility that deletions involving *ERCC5* may contribute to melanoma genesis in the setting of chronic sun damage. Overall, this comparative analysis suggested that, in aggregate, cultured melanoma collections might provide a genetically appropriate model system for systematic functional genomic characterization.

Integration of significant genomic lesions with melanoma gene expression data.

Although the majority of GISTIC peaks pinpointed genomic regions implicated previously in melanoma (refs. 20, 32, 33; Supplementary Fig. S1A), in most cases the relevant effector genes remain unknown. To identify candidate genes targeted by the GISTIC lesions, we systematically partitioned our data set into two classes based on the presence or absence of the relevant GISTIC lesion and used the resulting classes to carry out SAM analysis of sample-matched gene expression data (see Materials and Methods). In principle, amplified genes that exhibit significantly up-regulated expression may denote candidate oncogene targets, whereas those within regions of deletion that show significant down-regulation may exert tumor suppressor mechanisms.

The results of this genome-wide SAM analysis are shown in Tables 1 and 2. In several instances, a short list of differentially expressed genes was identified whose cellular functions suggested plausible cancer mechanisms. For example, we identified five up-regulated genes from the 15q26 GISTIC region that included *IQGAP1* (Table 1), which encodes a GTPase-activating protein that modulates RAC1/cdc42-mediated cellular adhesion (34). Similarly, four up-regulated genes from the GISTIC locus at 22q13 included the *EP300* gene (Table 1), which encodes a key transcriptional coactivator that cooperates with numerous cancer-associated factors, including microphthalmia-associated transcription factor (MITF; ref. 35). Several known or candidate melanoma tumor suppressors were also suggested by this analysis (Table 2), including *PTEN* (10q23) and *KLF6* (10p15; described below). Thus, combined analyses of sample-matched, genome-scale data posit multiple candidate tumorigenic mechanisms enacted by melanoma genomic aberrations.

Genome-wide measurements of LOH in melanoma.

High-density SNP arrays also enable inference of LOH (36), even in the absence of matched normal DNA (23). To identify significant LOH regions within our cultured melanoma collection, we predicted LOH patterns within each sample using a hidden Markov model (23), and applied the GISTIC algorithm to the resulting LOH segments (see Materials and Methods). A strong concordance was observed between regions of LOH and copy loss (Fig. 1C), suggesting that most melanoma LOH events occur by hemizygous deletion. The major exceptions to this pattern occurred at chromosomes 5q and 17p, where LOH in the absence of significant hemizygous deletion (“copy-neutral” LOH) was apparent. Although the relevant tumor suppressor at chromosome 5q has not been identified, the LOH peak at chromosome 17p centers on the well-known *TP53* tumor suppressor gene (Fig. 1C). This suggests that copy-neutral LOH may represent an important mechanism of p53 inactivation in melanoma. In a subset of short-term culture samples, a segment of chromosome 4q

contained hemizygous deletion but limited LOH (Fig. 1C). This unusual phenomenon, which could potentially be explained by copy loss and biallelic retention in the setting of hyperploid tumors, implies that this region of the melanoma genome might be relatively refractory to LOH or uniparental disomy.

Molecular classification of melanoma based on chromosomal aberrations.

We next sought to determine if significant chromosomal events might organize the melanoma samples into molecularly distinct and/or biologically relevant subsets. To address this, we applied established unsupervised learning methods (37, 38) to the lesions identified by GISTIC (see Materials and Methods). As shown in Fig. 2, hierarchical clustering grouped GISTIC-annotated cultured melanoma samples into six main branches. Two major subclusters (clusters 4 and 5) were characterized by the presence of chromosome 7p/7q gains (P = 1.1e–05, P = 2.5e–05, two-tailed Fisher's exact test) and chromosome 10 losses (P = 7.9e–4, P = 6.5e–05) with cluster 5 being enriched for additional alterations, most notably gains on chromosome 22q (P = 1.4e-3). These clusters were associated with an enrichment of BRAF mutation compared with NRAS mutation (P = 4.7e-3, two-tailed Fisher's exact test; Fig. 2), thereby highlighting the observation that in a subset of samples mutated *BRAF* is amplified, at least to low levels, in melanoma (Supplementary Fig. S3C–E). Another prominent subcluster (cluster 6) was largely defined by a relative paucity of chromosome 10 losses when compared with clusters 1 to 5. Interestingly, although 7q gains were relatively common in this terminal branch, the prevalence of BRAF(V600E) mutation was diminished compared with clusters 4 and 5, raising the possibility of an additional target(s) of 7q copy gains in melanoma. In contrast, clusters 1 and 2 exhibited a reciprocal pattern, with chromosome 10 losses characteristic of both branches. Overall, these results suggested that clustering GISTIC lesions may provide biologically relevant molecular groupings of melanoma tumor samples.

Predicting genes targeted by nonfocal chromosome 10 deletions in melanoma.

In melanoma, as in many solid tumors, most statistically significant chromosomal aberrations span large genomic regions whose target genes are unknown (20, 32, 33). Among many other lesions, this pattern is exemplified by the gains and losses involving chromosomes 7 and 10, respectively, two prominent drivers of the GISTIC-based melanoma subclusters described above. Although one of the most significantly "amplified" regions on chromosome 7 centers at 7q34 (contains *BRAF*; Fig. 1A), most chromosome 10 copy losses cover the entire chromosome, punctuated by a more focal GISTIC peak at 10q23.31 (Fig. 1B; Supplementary Fig. S1A and B) spanning the *PTEN* tumor suppressor gene. These initial observations are consistent with a model in which chromosome 7 gains and chromosome 10 deletions enhance oncogenic BRAF and diminish PTEN expression, thereby suggesting cooperating effects of these two cancer genes in melanoma, as previously suggested (39). On the other hand, whereas broad chromosome 10 deletions are highly prevalent even in early-stage primary melanomas (ref. 20; Fig. 1B), the relative contribution of PTEN inactivation in melanoma establishment remains unclear.

To investigate this, we examined the extent to which panchromosome 10 deletions were associated with functional PTEN inactivation, either through genetic mutation or mRNA/

protein loss. As shown in Fig. 3A, 5 of 42 short-term cultures and cell lines harboring large chromosome 10 losses also contained focal *PTEN* homozygous deletions; similar results were observed in an independent melanoma cell line panel previously described (Supplementary Fig. S3A). However, consistent with prior DNA sequencing analyses of short-term melanoma cultures and primary tumors (40, 41), only 8 of 78 lines examined by sequencing contained inactivating *PTEN* mutations; of these samples, only 5 also harbored hemizygous loss and LOH of chromosome 10. Using sample-matched gene expression data, we then examined PTEN mRNA expression in relation to genomic deletion. Here, whereas *PTEN* homozygous deletion correlated with a marked reduction in PTEN expression, <50% of samples with hemizygous deletions exhibited decreased PTEN levels when compared with samples without alterations at this locus (Fig. 3B). Similar results were observed following immunoblot analysis of PTEN protein levels in a subset of samples (Fig. 3C). Although tempered by the incomplete sensitivity to detect small-scale deletions at the *PTEN* locus, these observations raised the possibility that an as yet uncharacterized tumor suppressor gene(s) located on chromosome 10 might contribute to melanoma establishment in addition to *PTEN*.

To identify candidate tumor suppressor genes enacted by nonfocal chromosome 10 deletions in an unbiased manner, we partitioned 66 matched samples into tertiles based on the ranked magnitude of chromosome 10 loss (see Materials and Methods) and segregated the two extreme tertiles according to the class distinction “chromosome 10-deleted” (22 samples) versus “chromosome 10-wild-type” (22 samples). We then carried out a genome-wide significance analysis (SAM) using sample-matched gene expression data, as described above. As shown in Fig. 3D, 43 unique transcripts exhibited significantly diminished expression in association with chromosome 10 deletion at a δ value of 1.4673 (median false number of genes = 0). Interestingly, two chromosome 10 genes with putative tumor suppressor roles—*CUL2* (chromosome 10p11) and *KLF6* (chromosome 10p15)—scored even more highly than *PTEN* in this analysis (Fig. 3D; Supplementary Fig. S6). *CUL2* encodes a cullin protein whose yeast homologues negatively regulate the cell cycle (42) and also forms an E3 ubiquitin ligase complex with the von Hippel-Lindau tumor suppressor protein (43, 44). *KLF6* encodes a zinc finger transcription factor implicated as a tumor suppressor in several malignancies (45–47). Notably, the *KLF6* locus was also identified as significantly deleted by GISTIC analysis (Table 2). Thus, *CUL2* and *KLF6* represent intriguing candidate melanoma tumor suppressor genes targeted by chromosome 10 deletions.

Modifiers of RAF/mitogen-activated protein kinase/extracellular signal–regulated kinase kinase dependency in melanoma.

The establishment of an experimentally tractable system reflective of melanoma genomic diversity provides a means to identify molecular predictors and modifiers of therapeutic response in this highly chemoresistant malignancy. Because most cutaneous melanomas harbor activating point mutations in BRAF or NRAS (30, 48)—two key effectors of the mitogen-activated protein (MAP) kinase signaling cascade—several ongoing clinical trials are investigating the efficacy of RAF and MAP kinase/extracellular signal–regulated kinase (ERK) kinase (MEK) inhibitors in this setting. To identify genetic/molecular modifiers of

MAP kinase dependency that might influence therapeutic response, we examined cellular response to pharmacologic MAP kinase inhibition in a panel of 31 short-term cultures using the MEK inhibitor CI-1040. $BRAF^{V600E}$ mutation was invariably associated with sensitivity to MEK inhibition, as previously shown (ref. 9; e.g., submicromolar CI-1040 GI_{50} values; Fig. 4A and Supplementary Fig. S4), although one $BRAF^{V600E}$ line (WM853-2) was moderately less sensitive to CI-1040. In contrast, NRAS-mutant melanomas exhibited highly variable MAP kinase dependencies; whereas four NRAS-mutant lines with codon 61 mutations showed CI-1040 sensitivity patterns similar to the $BRAF^{V600E}$ panel, two lines harboring codon 12/13 NRAS mutations were “indifferent” to CI-1040 treatment. PTEN protein loss was more common in lines showing decreased sensitivity to CI-1040 (Fig. 4A), although this trend did not reach statistical significance. Surprisingly, a short-term culture harboring the $BRAF^{K601E}$ mutation also showed insensitivity to CI-1040. Together, these data suggested the presence of additional genetic or molecular modifiers of melanoma MAP kinase dependency apart from BRAF or NRAS mutation.

To investigate this in more detail, we examined the associated genomic and protein data in the melanoma lines described above. Despite the diversity of CI-1040 GI_{50} values, a similar degree of target inhibition was evident in several representative lines, as measured by p-ERK immunoblotting studies (Supplementary Fig. S4A). A genome-wide analysis of correlated chromosomal alterations and expressed genes (Supplementary Fig. S5) was unrevealing, encumbered by the relatively small CI-1040–insensitive sample size (three samples). However, two lines harboring the $FGFR1^{S125L}$ mutation exhibited markedly enhanced sensitivity to MEK inhibition when compared with the A375 control cell line (Fig. 4B). These data suggest that *FGFR1* mutations may provide an alternate (and independently druggable) means of eliciting a MAP kinase dependency in melanoma.

In contrast, “steady-state” immunoblot analyses of MEK and ERK found that p-ERK levels were markedly elevated in all CI-1040–insensitive lines (Fig. 4C). These results suggested that insensitivity to MEK inhibition might be characterized by differential regulation of ERK activation. To explore this, we grouped the melanoma lines into two classes based on either high or low p-ERK levels (seven lines each; as defined by data in Fig. 4C) and examined the mean expression of several ERK-regulated genes known to mediate feedback regulation of MAP kinase signaling using sample-matched gene expression data. As shown in Fig. 4D, induction of feedback regulatory genes such as *DUSP6, SPRY2*, and *SPRY4* was readily detectable in the melanoma cells relative to a panel of normal melanocytes (4 lines); however, the levels of induction were comparable regardless of steady-state p-ERK levels. Together, these data raise the possibility that posttranscriptional and/or novel regulatory mechanisms may affect MAP kinase activation/dependency in melanoma, and that concomitant measurement of oncogene mutations and p-ERK levels may refine knowledge of melanoma patients likely to respond to targeted RAF or MEK inhibition.

Discussion

The unprecedented opportunities of cancer genomics also present new challenges to the identification of “target-able” tumor mechanisms. For example, distinguishing causal from passenger alterations requires analytic approaches capable of transcending technology

platform limitations. Moreover, characterizing the downstream effectors of common genomic alterations requires tractable *in vitro* models reflective of these events. Our global genomic analyses indicate that melanoma short-term cultures seem to encompass the spectrum of essential genomic diversity present in primary cutaneous melanomas, suggesting that these may offer a robust platform for functional genomic characterization. Moreover, the high-resolution statistical delineations enabled by the GISTIC analytic framework strongly suggest (but do not prove) that such regions contain genes whose perturbation contributes to melanoma genesis or maintenance. Further, the availability of orthogonal genomic data sets such as gene expression profiles has helped to credential and prioritize several candidate effector genes for detailed functional study in relation to recurrent melanoma genomic changes.

Existing tumor genomic data sets have been generated using a variety of different technological platforms with widely divergent resolution and data output. This variation may pose a barrier to the types of cross-comparisons that might inform an overarching molecular taxonomy of cancer. In this regard, this study also exemplifies how GISTIC or related algorithms might overcome this bottleneck by providing a unifying analytic medium for comparative cancer genomics studies. As the number of genomically annotated tumor data sets continues to proliferate, this framework may facilitate systematic meta-analyses spanning large numbers of tumors and many diverse malignancies.

These analytic refinements also call renewed attention to instances where a full chromosome or chromosome arm displays a common tumor-associated alteration. In melanoma, deletions and LOH involving chromosome 10 provide an instructive example. Several previous studies have implicated inactivation of the *PTEN* tumor suppressor gene as a key (epi)genetic event in melanoma. Whereas the current study supports the notion that PTEN loss provides a driver alteration in some melanomas, it also suggests a model wherein broad chromosome 10 losses may enact a polygenic melanoma genesis mechanism(s) together with (or even apart from) PTEN inactivation. It should be noted, however, that none of the microarrays analyzed in this study have “tiling-level” resolution across the genome; thus, these platforms may be insensitive to the presence of “micro-genomic” deletions involving the *PTEN* locus (or other small-scale recurrent events). Nonetheless, the pervasive tendency toward large chromosomal perturbations in cancer underscores the future need for systematic functional studies in genetically characterized tumor model systems.

Application of hierarchical clustering to a matrix of (GISTIC-derived) significant genomic lesions yields melanoma subclasses whose characteristics are suggestive of mechanistic relevance. When applied broadly in cancer genomics, these analyses may help reduce the complexity of cancer genome aberrations while also laying a robust groundwork for molecular classification and downstream functional approaches. In the future, genetically annotated melanoma lines could be subjected to systematic RNA interference studies informed by GISTIC or related statistical information. Genes located within statistically credentialed genomic regions whose knockdown modulates a cancer phenotype of interest may illuminate druggable cellular pathways linked to tumor genomic events identifiable *in situ*.

Finally, cell culture models reflective of *in vivo* tumor genetic diversity offer an attractive avenue to identify molecular features that modify the efficacy of therapeutic agents. In melanoma, the MAP kinase pathway is commonly activated by BRAF or NRAS oncogene point mutations, and BRAF(V600E) mutation is associated with sensitivity to RAF or MEK inhibition. The data presented here suggest that in some contexts, NRAS or FGFR1 mutations may also confer sensitivity to MAP kinase pathway inhibition, but that high p-ERK may correlate with insensitivity to these inhibitors. Whereas these observations require detailed experimental followup, they show how cultured cell models facilitate orthogonal analyses of genomic and protein data to yield new insights into targeted therapeutic response. Overall, the large-scale application of these approaches to genetically annotated cancer cell culture models should provide a rich framework for extraction of key dependencies from tumor genomic data, thereby offering new therapeutic possibilities in melanoma and many other solid tumors.

Supplementary Material

Refer to Web version on PubMed Central for supplementary material.

Grant support:

The Swiss National Science Foundation grant 32-63704.00; Gottfried and Julia Bangerter Rhyner Stiftung; Genentech, Inc.; National Cancer Institute grants K08CA115927 and P50CA93683; the Burroughs-Wellcome Fund; and the Robert Wood Johnson Foundation. T.R. Golub is an investigator of the Howard Hughes Medical Institute.

References

1. Vogelstein B, Kinzler KW. Cancer genes and the pathways they control. Nat Med 2004;10:789–99. [PubMed: 15286780]
2. Weber BL. Cancer genomics. Cancer Cell 2002;1:37–47. [PubMed: 12086886]
3. Kantarjian H, Sawyers C, Hochhaus A, et al. Hematologic and cytogenetic responses to imatinib mesylate in chronic myelogenous leukemia. N Engl J Med 2002;346:645–52. [PubMed: 11870241]
4. Demetri GD, von Mehren M, Blanke CD, et al. Efficacy and safety of imatinib mesylate in advanced gastrointestinal stromal tumors. N Engl J Med 2002;347:472–80. [PubMed: 12181401]
5. Paez JG, Janne PA, Lee JC, et al. EGFR mutations in lung cancer: correlation with clinical response to gefitinib therapy. Science 2004;304:1497–500. [PubMed: 15118125]
6. Lynch TJ, Bell DW, Sordella R, et al. Activating mutations in the epidermal growth factor receptor underlying responsiveness of non-small-cell lung cancer to gefitinib. N Engl J Med 2004;350:2129–39. [PubMed: 15118073]
7. Pao W, Miller V, Zakowski M, et al. EGF receptor gene mutations are common in lung cancers from “never smokers” and are associated with sensitivity of tumors to gefitinib and erlotinib. Proc Natl Acad Sci U S A 2004;101:13306–11. [PubMed: 15329413]
8. Garraway LA, Widlund HR, Rubin MA, et al. Integrative genomic analyses identify MITF as a lineage survival oncogene amplified in malignant melanoma. Nature 2005;436:117–22. [PubMed: 16001072]
9. Solit DB, Garraway LA, Pratilas CA, et al. BRAF mutation predicts sensitivity to MEK inhibition. Nature 2006;439:358–62. [PubMed: 16273091]
10. Bild AH, Yao G, Chang JT, et al. Oncogenic pathway signatures in human cancers as a guide to targeted therapies. Nature 2006;439:353–7. [PubMed: 16273092]
11. Neve RM, Chin K, Fridlyand J, et al. A collection of breast cancer cell lines for the study of functionally distinct cancer subtypes. Cancer Cell 2006;10:515–27. [PubMed: 17157791]

12. Potti A, Mukherjee S, Petersen R, et al. A genomic strategy to refine prognosis in early-stage non-small-cell lung cancer. N Engl J Med 2006;355:570–80. [PubMed: 16899777]
13. Miller AJ, Mihm MC Jr. Melanoma. N Engl J Med 2006;355:51–65. [PubMed: 16822996]
14. Chin L, Garraway LA, Fisher DE. Malignant melanoma: genetics and therapeutics in the genomic era. Genes Dev 2006;20:2149–82. [PubMed: 16912270]
15. Fountain JW, Karayiorgou M, Ernstoff MS, et al. Homozygous deletions within human chromosome band 9p21 in melanoma. Proc Natl Acad Sci U S A 1992;89:10557–61. [PubMed: 1438246]
16. Pavey S, Johansson P, Packer L, et al. Microarray expression profiling in melanoma reveals a BRAF mutation signature. Oncogene 2004;23:4060–7. [PubMed: 15048078]
17. Tsao H, Zhang X, Fowlkes K, Haluska FG. Relative reciprocity of NRAS and PTEN/MMAC1 alterations in cutaneous melanoma cell lines. Cancer Res 2000;60:1800–4. [PubMed: 10766161]
18. Thomas RK, Baker AC, Debiasi RM, et al. High-throughput oncogene mutation profiling in human cancer. Nat Genet 2007;39:347–51. [PubMed: 17293865]
19. Lamb J, Crawford ED, Peck D, et al. The Connectivity Map: using gene-expression signatures to connect small molecules, genes, and disease. Science 2006;313:1929–35. [PubMed: 17008526]
20. Curtin JA, Fridlyand J, Kageshita T, et al. Distinct sets of genetic alterations in melanoma. N Engl J Med 2005;353:2135–47. [PubMed: 16291983]
21. Hupe P, Stransky N, Thiery JP, Radvanyi F, Barillot E. Analysis of array CGH data: from signal ratio to gain and loss of DNA regions. Bioinformatics 2004;20:3413–22. [PubMed: 15381628]
22. Beroukhim R, Getz G, Nghiemphu L, et al. Assessing the significance of chromosomal aberrations in cancer: methodology and application to glioma. Proc Natl Acad Sci U S A 2007;104:20007–12. [PubMed: 18077431]
23. Beroukhim R, Lin M, Park Y, et al. Inferring loss-of-heterozygosity from unpaired tumors using high-density oligonucleotide SNP arrays. PLoS Comput Biol 2006;2:e41. [PubMed: 16699594]
24. Eisen MB, Spellman PT, Brown PO, Botstein D. Cluster analysis and display of genome-wide expression patterns. Proc Natl Acad Sci U S A 1998;95:14863–8. [PubMed: 9843981]
25. Reich M, Liefeld T, Gould J, Lerner J, Tamayo P, Mesirov JP. GenePattern 2.0. Nat Genet 2006;38:500–1. [PubMed: 16642009]
26. Tusher VG, Tibshirani R, Chu G. Significance analysis of microarrays applied to the ionizing radiation response. Proc Natl Acad Sci U S A 2001;98:5116–21. [PubMed: 11309499]
27. Bignell GR, Huang J, Greshock J, et al. High-resolution analysis of DNA copy number using oligonucleotide microarrays. Genome Res 2004;14:287–95. [PubMed: 14762065]
28. Zhao X, Li C, Paez JG, et al. An integrated view of copy number and allelic alterations in the cancer genome using single nucleotide polymorphism arrays. Cancer Res 2004;64:3060–71. [PubMed: 15126342]
29. Weir BA, Woo MS, Getz G, et al. Characterizing the cancer genome in lung adenocarcinoma. Nature 2007;450:893–8. [PubMed: 17982442]
30. Davies H, Bignell GR, Cox C, et al. Mutations of the BRAF gene in human cancer. Nature 2002;417:949–54. [PubMed: 12068308]
31. Hussussian CJ, Struewing JP, Goldstein AM, et al. Germline p16 mutations in familial melanoma. Nat Genet 1994;8:15–21. [PubMed: 7987387]
32. Jonsson G, Dahl C, Staaf J, et al. Genomic profiling of malignant melanoma using tiling-resolution arrayCGH. Oncogene 2007;26:4738–48. [PubMed: 17260012]
33. Stark M, Hayward N. Genome-wide loss of heterozygosity and copy number analysis in melanoma using high-density single-nucleotide polymorphism arrays. Cancer Res 2007;67:2632–42. [PubMed: 17363583]
34. Hart MJ, Callow MG, Souza B, Polakis P. IQGAP1, a calmodulin-binding protein with a rasGAP-related domain, is a potential effector for cdc42Hs. EMBO J 1996;15:2997–3005. [PubMed: 8670801]
35. Price ER, Ding HF, Badalian T, et al. Lineage-specific signaling in melanocytes. C-kit stimulation recruits p300/CBP to microphthalmia. J Biol Chem 1998;273:17983–6. [PubMed: 9660747]

36. Lindblad-Toh K, Tanenbaum DM, Daly MJ, et al. Loss-of-heterozygosity analysis of small-cell lung carcinomas using single-nucleotide polymorphism arrays. Nat Biotechnol 2000;18:1001–5. [PubMed: 10973224]
37. Duda RO, Hart PE, Stork DG. Pattern classification. 2nd ed. New York: Wiley-Interscience; 2000.
38. Quackenbush J. Microarray analysis and tumor classification. N Engl J Med 2006;354:2463–72. [PubMed: 16760446]
39. Tsao H, Goel V, Wu H, Yang G, Haluska FG. Genetic interaction between NRAS and BRAF mutations and PTEN/MMAC1 inactivation in melanoma. J Invest Dermatol 2004;122:337–41. [PubMed: 15009714]
40. Pollock PM, Walker GJ, Glendening JM, et al. PTEN inactivation is rare in melanoma tumours but occurs frequently in melanoma cell lines. Melanoma Res 2002;12:565–75. [PubMed: 12459646]
41. Daniotti M, Oggionni M, Ranzani T, et al. BRAF alterations are associated with complex mutational profiles in malignant melanoma. Oncogene 2004;23:5968–77. [PubMed: 15195137]
42. Kipreos ET, Lander LE, Wing JP, He WW, Hedgecock EM. cul-1 is required for cell cycle exit in *C. elegans* and identifies a novel gene family. Cell 1996;85:829–39. [PubMed: 8681378]
43. Iwai K, Yamanaka K, Kamura T, et al. Identification of the von Hippel-Lindau tumor-suppressor protein as part of an active E3 ubiquitin ligase complex. Proc Natl Acad Sci U S A 1999;96:12436–41. [PubMed: 10535940]
44. Pause A, Lee S, Worrell RA, et al. The von Hippel-Lindau tumor-suppressor gene product forms a stable complex with human CUL-2, a member of the Cdc53 family of proteins. Proc Natl Acad Sci U S A 1997;94:2156–61. [PubMed: 9122164]
45. Kimmelman AC, Qiao RF, Narla G, et al. Suppression of glioblastoma tumorigenicity by the Kruppel-like transcription factor KLF6. Oncogene 2004;23:5077–83. [PubMed: 15064720]
46. Narla G, Heath KE, Reeves HL, et al. KLF6, a candidate tumor suppressor gene mutated in prostate cancer. Science 2001;294:2563–6. [PubMed: 11752579]
47. Kremer-Tal S, Reeves HL, Narla G, et al. Frequent inactivation of the tumor suppressor Kruppel-like factor 6 (KLF6) in hepatocellular carcinoma. Hepatology 2004;40:1047–52. [PubMed: 15486921]
48. van ’t Veer LJ, Burgering BM, Versteeg R, et al. N-ras mutations in human cutaneous melanoma from sun-exposed body sites. Mol Cell Biol 1989;9:3114–6. [PubMed: 2674680]
49. Futreal PA, Coin L, Marshall M, et al. A census of human cancer genes. Nat Rev Cancer 2004;4:177–83. [PubMed: 14993899]

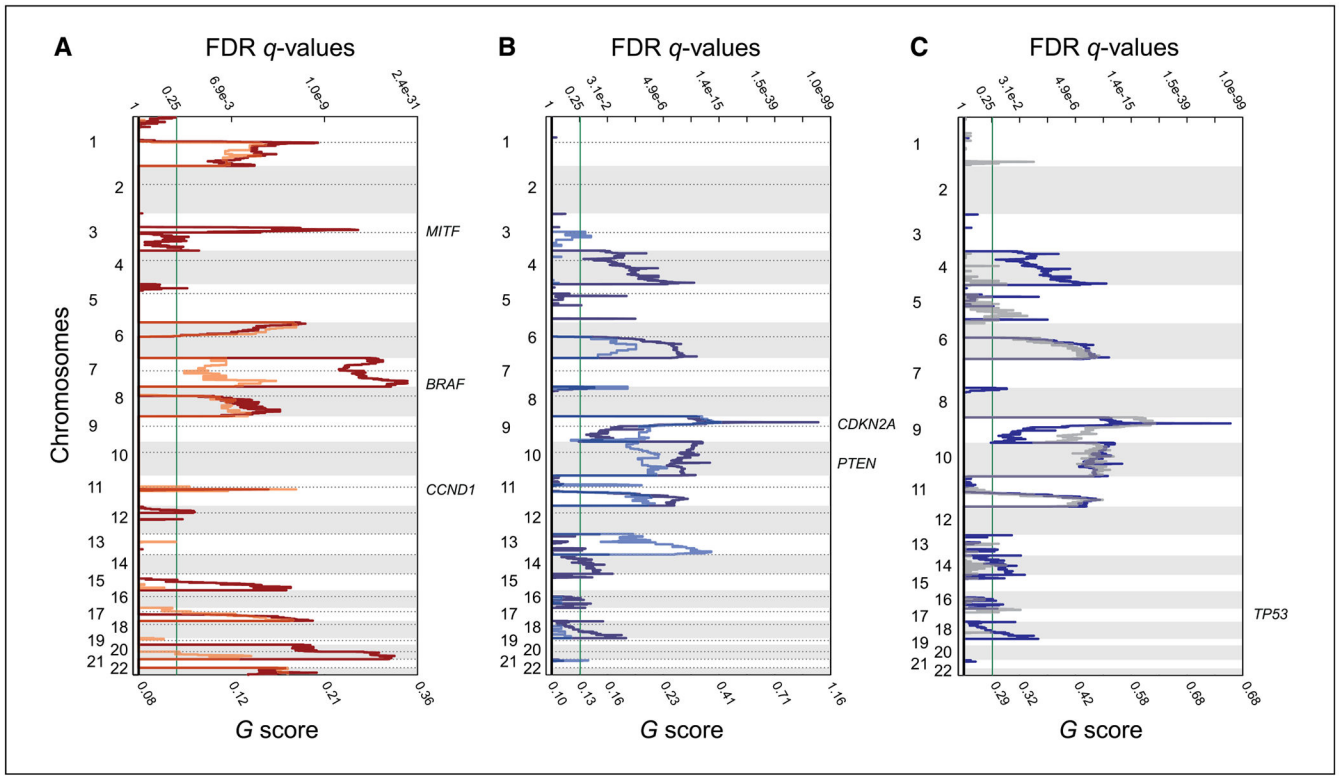

Figure 1.

Significant copy number and LOHalterations in melanoma. Statistically significant genomic amplifications (*A*) and deletions (*B*) pinpointed by GISTIC analysis of 101 cultured melanoma lines primarily from dermal metastases (*dark red* and *dark blue*, respectively) and 70 primary cutaneous melanomas (*orange* and *light blue*, respectively). *Top axis*, false discovery rate–corrected *q* values (threshold false discovery rate, 0.25; *green line*); *left axis*, chromosome; *bottom axis, G-score* (see text). *C*, GISTIC plot of inferred LOH (*gray*) is superimposed onto the chromosome deletion plot from *B* (*dark blue*) in cultured melanoma lines. Selected known melanoma oncogenes and tumor suppressors are indicated.

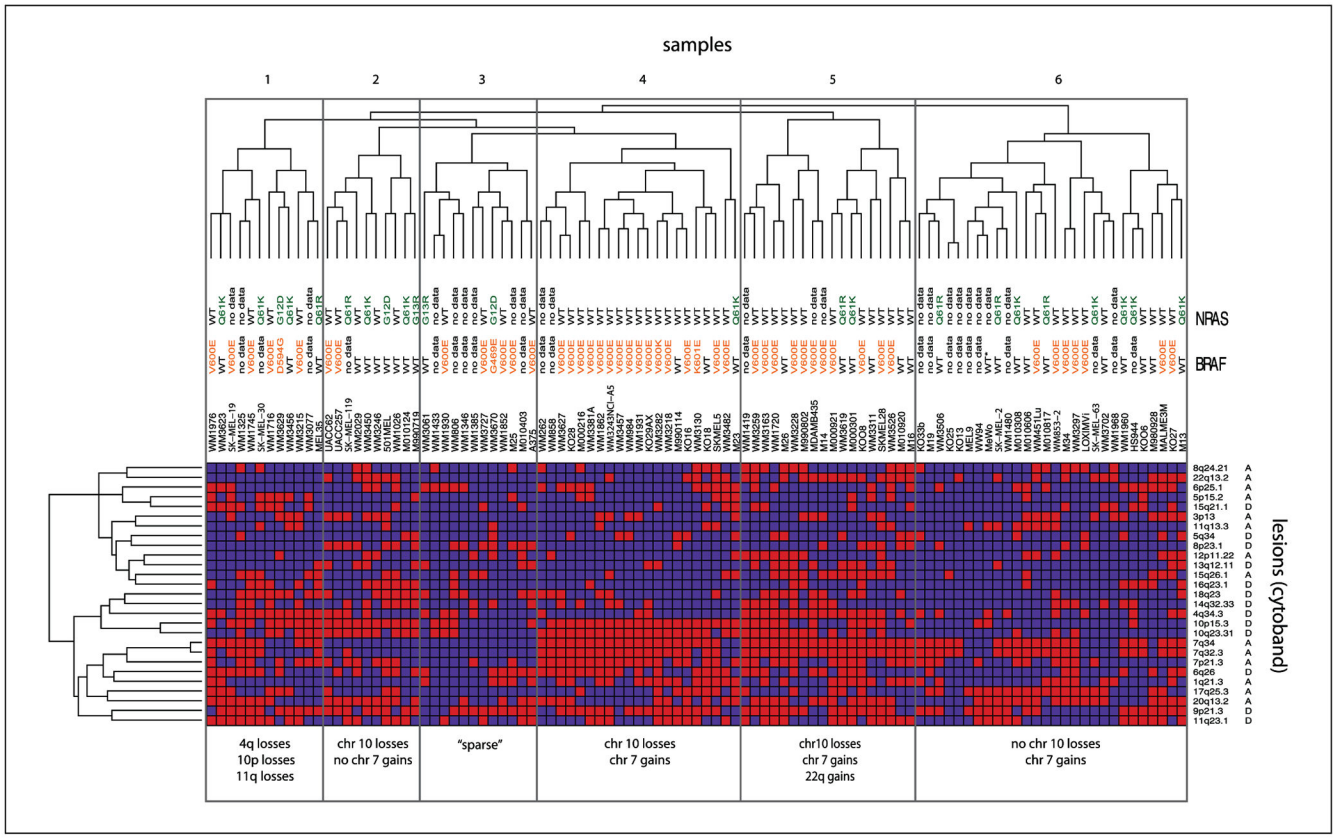

Figure 2.

Clustering analysis of significant melanoma genomic alterations. Hierarchical clustering of GISTIC lesions (discretized smoothed copy number; see Materials and Methods) by the Euclidean distance metric and complete linkage. *Rows*, genomic lesions identified by GISTIC algorithm (see text); *columns*, samples. *Red*, presence; *blue*, absence of lesions denoted by cytobands (*A*, amplification; *D*, deletion; *right*). Mutation status of BRAF and NRAS are noted above the matrix. Major clusters are indicated by boxes labeled 1 to 6.

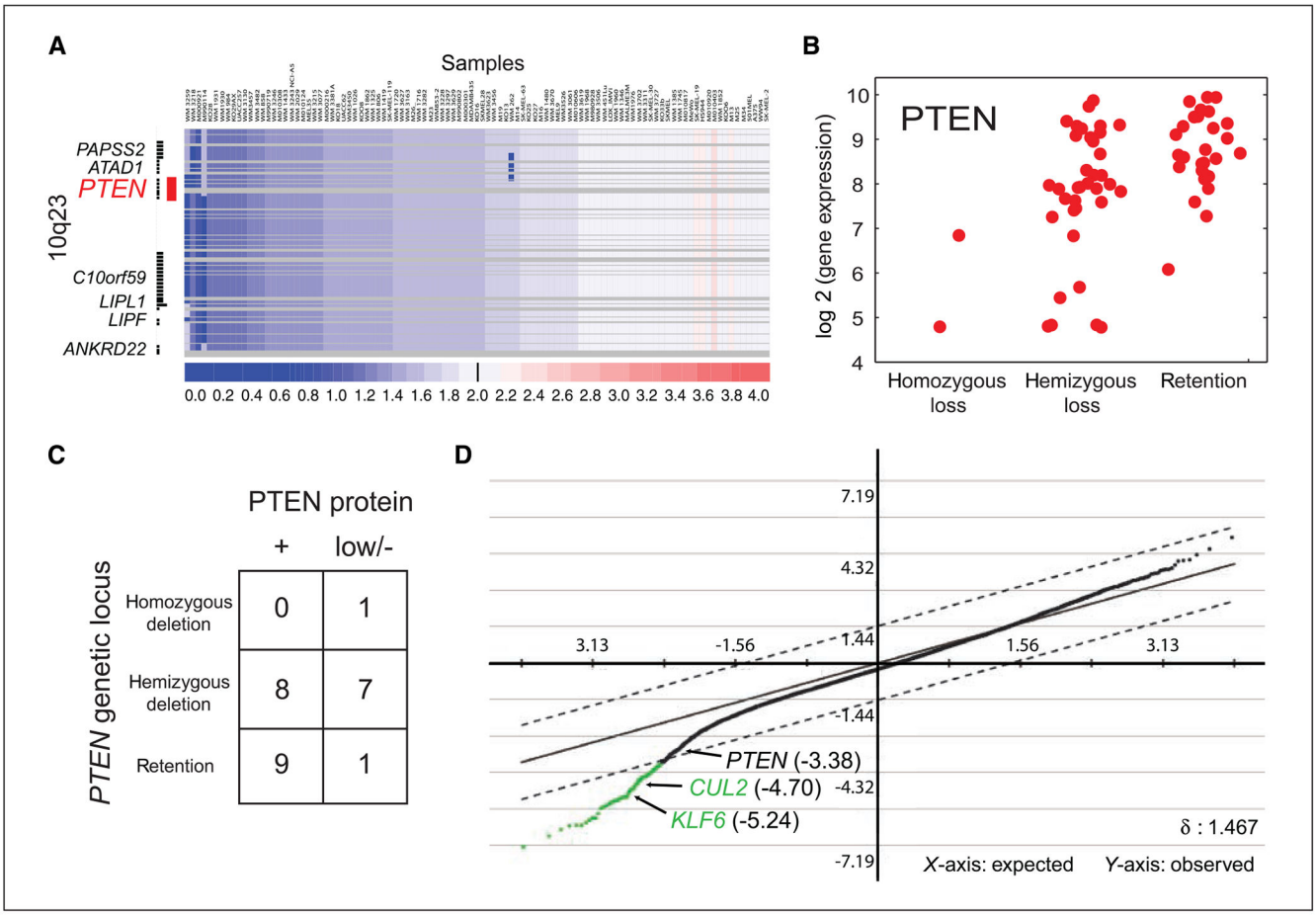

Figure 3.

Integrative analysis of chromosome 10 deletions in melanoma. *A*, heatmap view of smoothed 250K and 50K SNP array data spanning the *PTEN* locus (*red*, copy gains; *blue*, copy losses). Samples (*columns*) are sorted based on copy number values derived from segmented data. *B, PTEN* gene expression values stratified according to homozygous deletion, hemizygous loss, or retention of the underlying locus. *C*, summary of PTEN protein levels in relation to chromosomal deletions affecting the *PTEN* locus. *D*, significance analysis of melanoma gene expression data. Samples are stratified according to loss or retention at chromosome 10 (see Materials and Methods). The positions of *CUL2, KLF6*, and *PTEN* are shown.

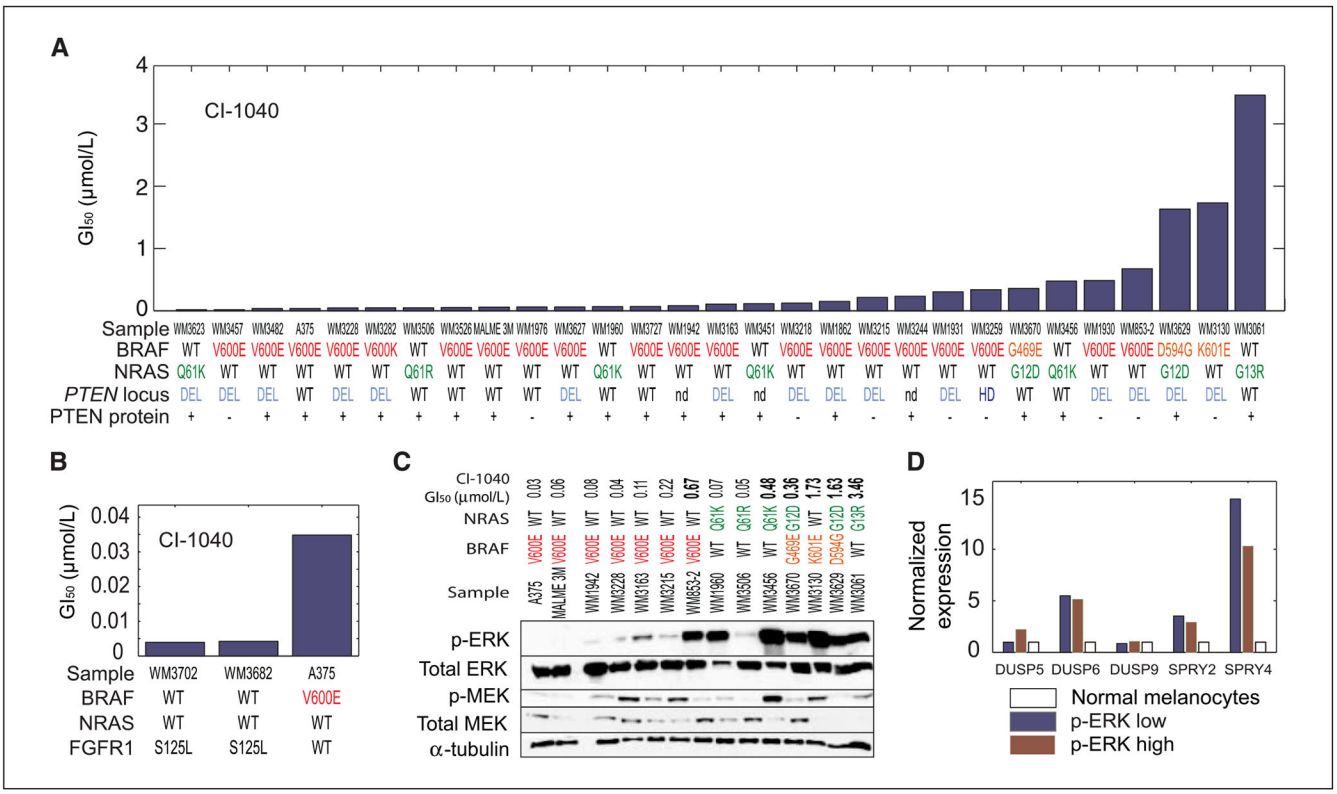

Figure 4.

Molecular modifiers of MAP kinase dependency in melanoma. *A*, pharmacologic GI_{50} values for the MEK inhibitor CI-1040. Mutation status for *BRAF* and *NRAS* genes, genomic status at the *PTEN* locus, and PTEN protein levels are indicated. *B*, GI_{50} values for two short-term cultures harboring FGFR1 mutations are shown alongside a control melanoma cell line (A375). *C*, Western blot analyses of p-ERK, total ERK, p-MEK, total MEK, and α-tubulin are shown for selected melanoma lines (CI-1040 GI_{50} values are indicated). *D*, relative expression of MAP kinase feedback regulatory genes in melanoma lines with low or high p-ERK levels in relation to normal melanocytes.

Table 1.

Significant regions of chromosomal copy gain in melanoma

Chromosome	Cytoband	*Q* value	GISTIC peak (Mb)	Genes in region	Candidate genes
1	1q21.3	6.10e—09	chr1:147.2-149.2	53	*ARNT*, ***CDC42SE1, ECM1, ENSA FAM63A, LASS2,****MLLT11*, ***MRPL9, PIK4CB, PIP5K1A, POGZ, PRUNE,PSMB4, PSMD4, RFX5, SETDB1, TARSL1*** [36 NS genes]
3	3p13	9.36e—17	chr3:69.87-70.22	1	*MITF*
5	5p15.33	1.37e—01	chr5:1e-6-1.680	3	*CTNND2, DNAH5, TRIO*
6	6p25.1	5.70e—08	chr6:4.07-5.62	9	*C6orf146, C6orf201, CDYL, FARS2, KU-MEL-3, LYRM4, PECI,* ***PRPF4B****, RPP40*
7	7p21.3	2.78e—20	chr7:12.1-13.1	2	*ARL4A, SCIN*
7	7q32.3	1.18e—27	chr7:129.6-130.4	6	*COPG2, CPA1, KLF14, MEST, TSGA1, TSGA14*
7	7q34	5.07e—26	chr7:139.03-140.48	12	*BRAF*, ***MKRN1, NDUFB2*** [9 NS genes]
8	8q24.21	1.73e—05	chr8:121.7-129.0	33	*MYC*, ***RNF139, C8orf32, DERL1, WDR67*** [28 NS genes]
11	11q13.3	1.02e—04	chr11:69.0-69.8	7	*FLJ42258, FGF4, FADD, FGF19, FGF3 TMEM16A, CCND1*, *ORAOV1*
12	12p11.22	9.90e—02	chr12:24.3-32.9	44	***DDX11, DNM1L, FAM60A, KRAS*** *, ***MRPS35, YARS2*** [38 NS genes]
15	15q26.1	2.63e—06	chr15:87.5-89.1	24	***AP3S2, IDH2, IQGAP1, POLG*** [20 NS genes]
17	17q25.3	2.25e—08	chr17:74.7-77.1	25	*KIAA1618*, ***MGC15523, TBC1D16*** [22 NS genes]
20	20q13.2	1.75e—23	chr20:49.1-50.5	4	*ATP9A, NFATC2, SALL4, ZFP64*
22	22q13.2	8.32e—09	chr22:39.7-40.9	28	***EP300*** *, ***NAGA PMM1*** [25 NS genes]

NOTE: Bold font denotes significant differentially expressed genes by whole-genome SAM analysis (median false genes = 0; see text). NS denotes genes in the region whose differential expression is not significant based on SAM analysis (see Supplementary Materials for full gene list).

*Known cancer gene (49).

Table 2.

Significant regions of chromosomal copy loss in melanoma

Chromosome	Cytoband	*Q* value	GISTIC peak (Mb)	Genes in region	Candidate genes
4	4q34.3	2.94e—10	chr4:182.5-182.9	0	—
5	5q34	1.03e—03	chr5:165.8-166.3	0	—
6	6q26	1.04e—10	chr6:162.4-163.7	2	*PACRG, PARK2*
8	8p23.1	9.27e—02	chr8:6.3-9.4	29	[29 NS genes]
9	9p21.3	1.59e—81	chr9:22.0-22.1	0	*CDKN2A*[*], *CDKN2B10*
10	10q23.31	2.14e—13	chr10:89.4-90.0	3	*ATAD1, PAPSS2,* ***PTEN***[*]
10	10p15.3	7.86e—12	chr10:2.5-4.1	3	***KLF6***[*], *PFKP, PITRM1,*
11	11q23.1	3.43e—09	chr11:111.2-112.0	15	[15 NS genes]
13	13q12.11	6.17e—02	chr13:19.9-90.5	204	***ALG5, C13orf23, CLN5, CRYL1, ESD, FNDC3A, KPNA3, MED4, MTMR6, MYCBP2, NUF1P1, P2RY5, RCBTB1, RNF6, RPL21, SAP18, SPG20, SUCLA2, TPT1*** [185 NS genes]
14	14q32.33	1.83e—02	chr14:102.3-103.9	18	***BAG5, C14orf2, MARK3*** [15 NS genes]
15	15q21.1	1.10e—01	chr15:41.6-43.3	27	***B2M, EIF3S1, ELL3, MFAP1, PDIA3, SERF2*** [21 NS genes]
16	16q23.1	1.23e—01	chr16:77.2-78.9	2	***MAF***[*], ***WWOX***
18	18q23	3.83e—03	chr18:62.7-76.2	34	***MBP, TXNL4A*** [32 NS genes]

NOTE: Bold font denotes significant differentially expressed genes by whole-genome SAM analysis (median false genes = 0; see text). NS denotes genes in the region whose differential expression is not significant based on SAM analysis (see Supplementary Materials for full gene list).

[*] Known cancer gene (49).